PCCP

Discovery of Twin Orbital-order Phases in Ferromagnetic Semiconducting VI3 Monolayer

Journal:	*Physical Chemistry Chemical Physics*
Manuscript ID	CP-ART-10-2019-005643.R1
Article Type:	Paper
Date Submitted by the Author:	20-Nov-2019
Complete List of Authors:	Huang, Chengxi; Nanjing University of Science and Technology, Applied Physics Wu, Fang; Nanjing Forestry University, Yu, Shunli; Nanjing University, National Laboratory of Solid State Microstructures and School of Physics Jena, Purusottam ; Virginia Commonwealth University, Physics Department Kan, Erjun; Nanjing University of Science and Technology,

Discovery of Twin Orbital-order Phases in Ferromagnetic Semiconducting VI_3 Monolayer

Chengxi Huang[ab], Fang Wu[c], Shunli Yu*[d], Puru Jena*[a], Erjun Kan*[b]

[a] Physics Department, Virginia Commonwealth University, Richmond, VA 23284

[b] Department of Applied Physics and Institution of Energy and Microstructure, Nanjing University of Science and Technology, Nanjing, Jiangsu 210094, P. R. China

[c] College of Information Science and Technology, Nanjing Forestry University, Nanjing, Jiangsu 210037, P. R. China

[d] National Laboratory of Solid State Microstructures and School of Physics, Nanjing University, Nanjing 210093, P.R. China

ABSTRACT: Spontaneous orbital symmetry breaking in crystals gives rise to abundant novel and interesting physical properties, which sometimes are concealed by the absence of geometrical distortions. We show that a recently discovered $3d^2$ system, namely the layered VI_3 ferromagnetic semiconductor, is a strongly correlated and orbital ordering system. Our analysis reveals that in a VI_3-like system there could be two types of orbital splitting, which are stabilized respectively by strong electronic correlation and inter-atomic exchange interactions. Consequently, on the basis of first-principles calculations, two competing low-energy phases of VI_3 monolayer (denoted as twin orbital-order phases) are discovered, in which the metal-insulator transition is driven by strong electronic correlation, and the orbital symmetry breaking is robust against geometrical distortions. Additionally, similar phenomena are also observed in other VI_3-like systems. These findings shed light on the unusual electronic behavior of a strongly correlated 2D system and will be interesting for nanoscale multi-functional spintronic applications.

Introduction

Symmetry breaking is a fundamental physical phenomenon in crystals. One of the well-known mechanisms of crystalline symmetry breaking is the Jahn-Teller (JT) effect, which widely exists in transition metal compounds and can be directly observed in experiment due to large geometrical distortions. JT effect is usually recognized as the origin of orbital symmetry breaking (i.e. orbital ordering in the case of a cooperative JT system), which gives rise to abundant interesting physical properties such as metal-insulator transitions[1], superconductivity[2], magnetostriction [3,4], ferroelectricity/multiferroicity[5-10] and electrically controllable phase transitions [11]. The other less explored mechanism deals with the occurrence of orbital symmetry breaking in the absence of geometrical distortions, in which case the exchange interactions and/or electronic correlations are considered to be responsible[12,13]. Thus, understanding the origin of orbital ordering is important for exploring metal-insulator transitions and magnetoelectric effects, especially in strongly correlated systems. However, it is generally difficult to determine which mechanism is dominant in a real system[14-16], because they are both enhanced by strong electronic correlations [17,18] and basically lead to identical symmetry breaking state. Consequently, despite the rapid development of the field of two-dimensional (2D) ferromagnetic and ferroelectric materials[19-22], the relations between orbital ordering and exchange interactions in a strongly correlated 2D system is still unclear.

Very recently, a new van der Waals (vdW) ferromagnetic (FM) semiconductor, i.e. VI_3, has been synthesized[23-25]. However, the observed low-temperature structural phases reported by different groups are controversial. Son *et al.* [25] claimed a $C2/c$ structure (in which the symmetry of a single layer is C_2) at ~ 40 K, while Tian *et al.* [24] reported a R-3 structure (in which the symmetry of a single layer is C_{3i}) at ~40 and ~60 K for VI_3 bulk. On the other hand, early first-principles studies reported a D_{3d} phase of the VI_3 monolayer, but the calculated electronic structure is metallic instead

of semiconducting.[26] Such controversies imply the possibility of an unusual electronic behavior yet to be revealed in the VI_3 system. Different from CrI_3 and $CrGeTe_3$ [27], the d^2 state of octahedrally coordinated V^{3+} ions may result in partially occupied threefold $t_{2g}\uparrow$ levels. Due to the narrow-band nature of 3*d* orbitals, an orbital splitting, possibly driven by JT distortion and/or exchange interaction, is expected to lift the electronic degeneracy and stabilize the system. Besides, the vdW layered VI_3 bulk can be easily exfoliated down to monolayers. These make the VI_3 monolayer an interesting platform to explore the orbital symmetry breaking and strongly correlated electronic behaviors in 2D systems.

In this work, on the basis of first-principles calculations, we demonstrate that the VI_3 monolayer indeed exhibits orbital symmetry breaking. JT distortion is subtle and not sufficient to explain the occurrence of orbital ordering and energy gap opening. Instead, the strong electronic correlation is found to be responsible. Interestingly, besides the local electronic correlation, the inter-atomic exchange interactions between adjacent V ions are found to be important and may lead to a different orbital splitting. As a result, two different orbital ordering phases of VI_3 monolayer are observed. The twin orbital-order phases are energetically nearly equivalent, but exhibit distinctly different magnetic and electronic properties. Our tight-binding analysis reveals that such unusual orbital symmetry breaking behaviors are determined by the edge-sharing octahedral geometry, which can be a general phenomenon in the VI_3-like 2D systems. This is also proved by our test calculations on other VI_3-like monolayers. Finally, we discuss the relationship between the twin orbital-order phases and the experimental observations of the properties of VI_3 bulk.

Method

Our first-principles calculations are based on density functional theory (DFT) implemented in the Vienna *Ab initio* Simulation Package (VASP)[28]. Generalized gradient approximation (GGA) for exchange-correlation functional given by Perdew,

Burke, and Ernzerhof (PBE)[29] is used. The projector augmented wave (PAW)[30] method is used to treat the core electrons. The spin-orbit coupling (SOC) effect was included in the self-consistent calculations with full relativistic pseudopotential. The plane wave cutoff energy is set to 500 eV and the first Brillouin zone is sampled by using a Γ-centered 12×12×1 Monkhorst-Pack[31] grid. The convergence criteria for energy and Hellmann-Feynman force component are set to be 1×10^{-6} eV and 0.002 eV/Å, respectively. The effective Hubbard U_{eff} = 3 eV is adopted for V-*d* orbitals according to Dudarev's method[32]. A test for different U_{eff} is also performed (Table S2 in the Supporting Information[33]). The phonon calculations are performed by using the PHONOPY code[37] combined with density functional perturbation theory method implemented in VASP. The maximally localized Wannier functions (MLWFs) are obtained by fitting a tight-binding Hamiltonian to the DFT electronic bands, as implemented in the Wannier90 package[34]. The V-*d* and I-*p* orbitals are adopted as projections to construct WFs. Appropriate inner and outer energy windows are used to perform the disentanglement procedure.

Results and Discussion

1. Tight-binding cluster model for VI_3-like systems

While early DFT study claimed a high-symmetric ($D_{3\mathrm{d}}$) metallic phase of VI_3 monolayer, recent experiments reported a large electronic band gap (> 0.8 eV) of VI_3. This implies a crystalline symmetry breaking of the $D_{3\mathrm{d}}$ phase. The first possibility that comes to mind is the classic JT effect. However, we find that the JT mechanism is not sufficient to explain the symmetry breaking for two reasons: i) The structural distortions of VI_3 is very subtle. For instance, in the experimentally observed *R*-3 structure, the V-I bond length difference is less than 0.004 Å and the I-V-I bond angle ranges from 86 to 93°. Thus, each V-I_6 unit is very close to an ideal octahedron. The resultant small crystal-field splitting of $t_{2\mathrm{g}}$ levels cannot explain the large energy gap opening. ii) In a d^2 octahedral system, the JT distortion usually prefers a stretching of

metal-ligand bonds along the z direction, which will result in a type-I splitting of t_{2g} levels (see Fig. 1a).[38] However, neither $C2/c$ nor R-3 structure exhibits this kind of distortion. Thus, the effect of electronic correlation and exchange interaction might become important and has to be considered in this case.

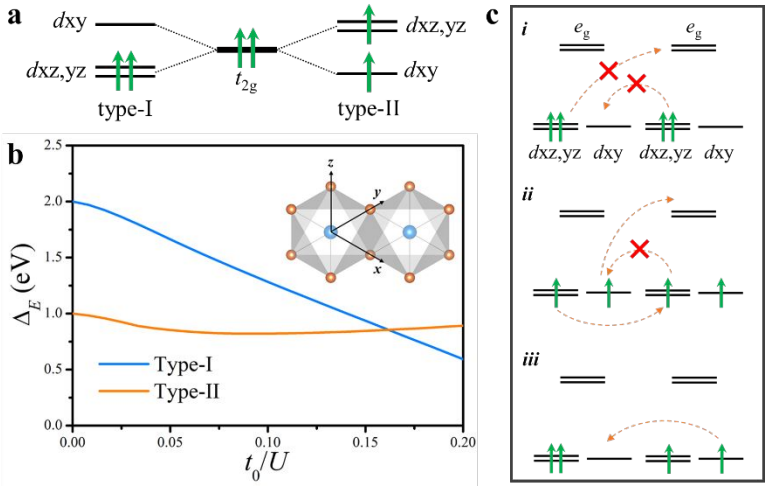

Fig. 1. (a) Rearrangement of on-site t_{2g} levels for type-I and type-II phases. (b) Electronic energy gains from type-I ($\Delta E = E_0 - E_{\text{type-I}}$, where E_0 represent the energy of the system without on-site splitting) and type-II ($\Delta E = E_0 - E_{\text{type-II}}$) splitting as a function of the ratio between hopping strength (t_0) and exchange field (U). Inset: the edge-sharing octahedral cluster model, in which the blue balls represent transition metal (V) ions, and the orange balls represent non-metal ligand ions. (c) Schematic diagrams of three possible occupation states in the absence of structural distortions, and corresponding effective exchange paths.

The intra-atomic exchange interaction (Hund's coupling) mainly affects the spin configuration at the atomic level to form a high-spin state, i.e. the S=1 state for d^2 V ion shown in Fig. 1, while it barely affects the orbital order. Thus, here we focus on the effect of inter-atomic exchange interactions. In a system with partially occupied

orbitals, although the on-site orbitals are energetically degenerate, one possible occupation state may gain more electronic energy from the inter-atomic exchange interactions than the others, leading to an orbital polarization or secondary splitting (if we take the on-site splitting, which is caused by JT distortion and/or electronic correlation, as the first splitting). To explore how inter-atomic exchange interactions affect the electronic structures of VI_3-like systems, here we construct a tight-binding based cluster model (see the inset in Fig. 1b) consisting of two edge-sharing octahedrons (see section II in the Supporting Information[33] for details). Each V ion is occupied by two electrons. Because VI_3 is experimentally proved to be FM, here we only consider the FM case. Without on-site splitting of t_{2g} orbitals, there will be three possible degenerate occupation states of the system (Fig. 1c). Next, we include the energy gain from inter-atomic exchange interactions, which is determined by the effective hopping between occupied and empty $d\uparrow$ orbitals. For case *i* (Fig. 1c), the energy gains are mainly from the $d$xz,yz↔e_g and $d$xz,yz↔$d$xy exchange interactions. By extracting the Slater-Koster hopping integrals[36], we find that both $d$xz,yz↔e_g and $d$xz,yz↔$d$xy effective hopping integrals are zero (see section II in the Supporting Information[33] for details). Thus, there is no exchange energy gains for this case. On the other hand, for case *ii*, large energy gains are expected from the nonzero $d$xy↔e_g and $d$xz,yz↔$d$xz,yz effective hopping. For case *iii*, the energy gains from $d$xy↔e_g and $d$xz,yz↔$d$xz,yz exchange interactions are smaller than that in case *b*, and the extra $d$xy↔$d$xy direct-exchange is usually weak compared with the super-exchange. Thus, an occupation state of case *ii* is preferred from the perspective of inter-atomic exchange interactions. Consequently, to further reduce the energy of the system, a type-II secondary splitting of t_{2g} levels (see Fig. 1a) may occur.

Above analysis shows that, in a VI_3-like system, the on-site splitting and inter-atomic exchange interactions may lead to different symmetry breaking phases (type-I or type-II), which is quite anomalous in comparison with previous studies. To

demonstrate this, we further calculated the energy of type-I and type-II phases by numerically diagonalizing the Hamiltonian matrix of the cluster model under mean-field approximation. The Hamiltonian of the cluster is written as[35]

$$\hat{H} = \sum_{i\alpha} \epsilon_{i\alpha} \hat{d}^{\dagger}_{i\alpha} \hat{d}_{i\alpha} + \sum_{k\gamma} \epsilon_{k\gamma} \hat{p}^{\dagger}_{k\gamma} p_{k\gamma} + \sum_{i\alpha,k\gamma} \left[T_{i\alpha,k\gamma} \hat{d}^{\dagger}_{i\alpha} p_{k\gamma} + h.c. \right] + \sum_{i\alpha,j\beta} \left[T_{i\alpha,j\beta} \hat{d}^{\dagger}_{i\alpha} \hat{d}_{j\beta} + h.c. \right] + \frac{U}{2} \sum_{i} \vec{e}_i \cdot \vec{S}_i,$$

where α (β) represent d orbitals ($d$xy, $d$yz, $d$xz, dx^2-y^2, dz^2), γ represents p orbitals (px, py, pz), i (j) represent site index of magnetic ions, k represents site of ligand ions, respectively. ϵ, T and U represent on-site energy, hopping integral and exchange field, respectively. Here we used a coefficient (t_0) to evaluate the strength of the inter-atomic exchange interactions between the neighboring V ions. When t_0 equals to zero, each V site is equivalent to an isolated JT molecule, thus the energy gains ($\Delta E = E_0 - E_{\text{type-I or type-II}}$, where E_0 is the energy of the system without on-site splitting) from type-I splitting is much larger than those from the type-II splitting, as shown in Fig. 1b. When the value of t_0/U (here $t_0 << U$) increases, the energy difference between type-I and type-II phases quickly decreases. And a crossing of the two profiles occur at $t_0/U \approx 0.16$, after which the type-II phase becomes more stable than the type-I phase. Note that, when t_0/U becomes very large (e.g. > 0.5), the ΔE for both type-I and type-II phase will be reduced to zero, which indicates that the $t_0 << U$ limit, namely the strong electronic correlation is important for the stabilization of both type-I and type-II phase. Overall, the above analysis reveals that different symmetry breaking phases of a VI_3-like system may occur depending on the strength of electronic correlation and inter-atomic exchange interactions.

2. Twin orbital-order phases of VI_3 monolayer

Next, we come back to the realistic VI_3 monolayer. We started our calculations from the high-symmetric D_{3d} phase of VI_3 monolayer using the DFT+U method with

U_{eff} ranging from 0 to 4 eV for V-*d* electrons. As expected, when $U_{\text{eff}} \geq 1$ eV, a soft phonon mode appears (Fig. 2a), which indicates a structural phase transition from high-symmetry to low-symmetry phase driven by strong electronic correlation. Interestingly, The vibration pattern of the soft phonon mode shows two possible deformation types (Fig. 2a). In type-I phase (Fig. 2b), the lateral lattice is slightly stretched along [110] orientation, whereas it is compressed in type-II phase (Fig. 2c). The optimized type-I and type-II structures both show reduced crystal symmetry, which is $C_{2\text{h}}$ and C_{s}, respectively. Note that, despite the small structural distortions, these two phases possess very different orbital orders and distinctly lower energies in comparison with the monolayers derived from the experimental bulk structures (i.e. C_2- and $C_{3\text{i}}$-VI_3 monolayers. See table S2 and Fig. S2 in the Supporting Information[33]).

The stabilization energy ($\Delta E = E_{D3\text{d}} - E_{\text{type-I or type-II}}$) significantly increases (from 0 to ~0.62 eV) as the value of U_{eff} increases (from 0 to 4 eV). When U_{eff} = 3 eV, ΔE is as large as ~0.51 eV. Apparently, such a large ΔE cannot be explained by small structural distortions. To make this more specific, we calculated the energy of an artificial state of VI_3 monolayer (type-I'), which possesses fixed $D_{3\text{d}}$ structure but the charge density of type-I phase (for type-II' case, the results are similar). The results show that the value of $E_{\text{D3d}} - E_{\text{type-I}'}$ (0.501 eV) is very close to that of $E_{\text{D3d}} - E_{\text{type-I}}$ (0.515 eV). These results suggest that the orbital symmetry breaking is insensitive to the structural distortion and is stabilized by strong electronic correlation.

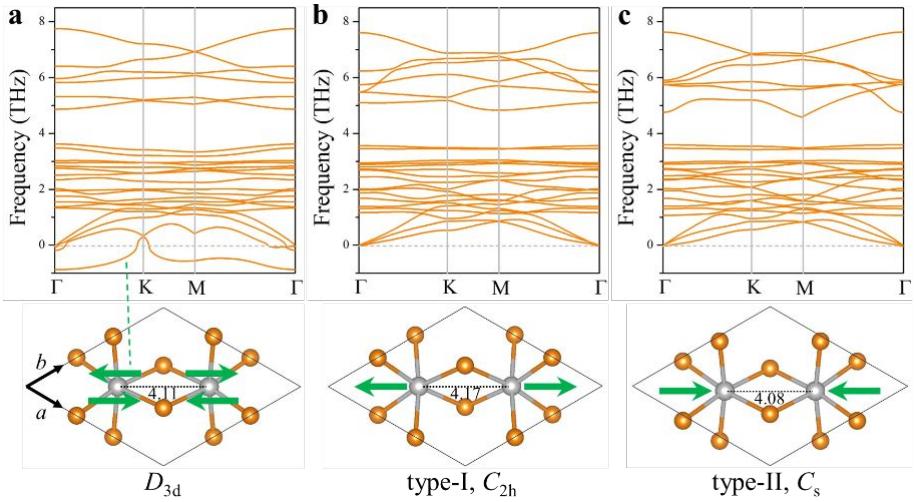

Fig. 2. (a) Phonon dispersion for VI_3 monolayer with fixed D_{3d} (undistorted) structure (upper panel) and the vibration mode of the V ions corresponding to the phonon band with imaginary frequency, i.e. soft phonon mode (lower panel). Phonon dispersions for VI_3 monolayer with optimized (b) type-I and (c) type-II structures. Gray and orange balls represent V and I ions, respectively. Green arrows represent the relative displacement directions of V ions. The inset labels represent the V-V bond lengths in angstrom.

To further investigate the origin of orbital symmetry breaking of the twin orbital-order phases, we examine their electronic structures. Different from the metallic D_{3d} phase (Fig. S3 in the Supporting Information[33]), both type-I and type-II phases are semiconducting with sizable electronic energy gaps (0.86 and 0.88 eV, respectively. See Fig. 3a and b). By extracting the MLWFs results (table S1 in the Supporting Information[33]), we find that the energy level splitting of the on-site t_{2g} orbitals for type-I and type-II phases are well-consistent with those predicted in the cluster model (Fig. 1a). This can also be clearly observed from the projected density of states (Fig. 3c and d) and the charge differences corresponding to the D_{3d} phase

(Insets in Fig. 3a and b), which show distinctly different rearrangements of t_{2g} levels and charge transfer behaviors for type-I and type-II phases.

Because of the D_{3d} symmetry the t_{2g} levels are not exactly degenerate but can inherently be divided into a doublet (*d*xz and *d*yz) and a singlet state (*d*xy). Thus, for type-I phase, the symmetry reduction from D_{3d} to C_{2h} caused by small structural distortion only slightly enlarges the splitting between the doublet and the singlet state. This can be confirmed from the MLWFs results, which show that the on-site splitting of type-I phase (1.41 eV) is a bit larger than that of type-I' phase (0.84 eV), but much larger than that of the D_{3d} phase (0.06 eV). Thus, the large energy gap opening and robust orbital ordering are mainly determined by the on-site splitting of t_{2g} levels due to strong electron correlation. For type-II phase, on the other hand, the orbital ordering is mainly a result of secondary splitting of t_{2g} levels driven by relatively strong inter-atomic exchange interactions. In this case, the energy gap opening is caused by the inter-orbital Coulomb interactions, which prohibit a simultaneous occupancy of *d*xz and *d*yz orbitals on one site (see Fig. S7 in the Supporting Information[33] for the evolution of V-*d* orbitals). Overall, the strong electron correlation is essential for the formation of both type-I and type-II phases. These imply that the VI_3 could be an FM Mott insulator.

More interestingly, our calculations show that the type-I and type-II phases are energetically nearly equivalent. Whether we use different value of U_{eff} or HSE06 functional, the calculated energy difference between these two phases is always less than 0.75 meV/atom (table S2 in the Supporting Information[33]). This indicates that the t_0/U value for VI_3 monolayer could be coincidentally located around the crossing point (Fig. 1b). Furthermore, we find that this energetic equivalency of twin orbital-order phases is robust against carrier doping and external strain (see Fig. S4 in the Supporting Information[33]). This suggests that the type-I and type-II phases might

have the same possibility of being synthesized in experiment; they may even simultaneously exist in a single VI_3 material as different domains.

In addition to the difference in electronic structures, the type-II phase shows an electric polarization whereas the type-I phase does not. In fact, the *d*xz and *d*yz orbitals in type-II phase are not exactly degenerate because of the C_s crystal symmetry. Consequently, a net electric dipole moment forms along the [-110] orientation, making the C_s-VI_3 monolayer a 2D ferroelectric material (if we take the thickness of the monolayer to be 6 Å, the polarization is ~0.78 $\mu C/cm^2$). But the ferroelectric switching barrier along [-110] orientation is quite small (~1.1 meV. See Fig. S5a in the Supporting Information[33]). Thus, the ferroelectric order of type-II phase can only exist at very low temperature.

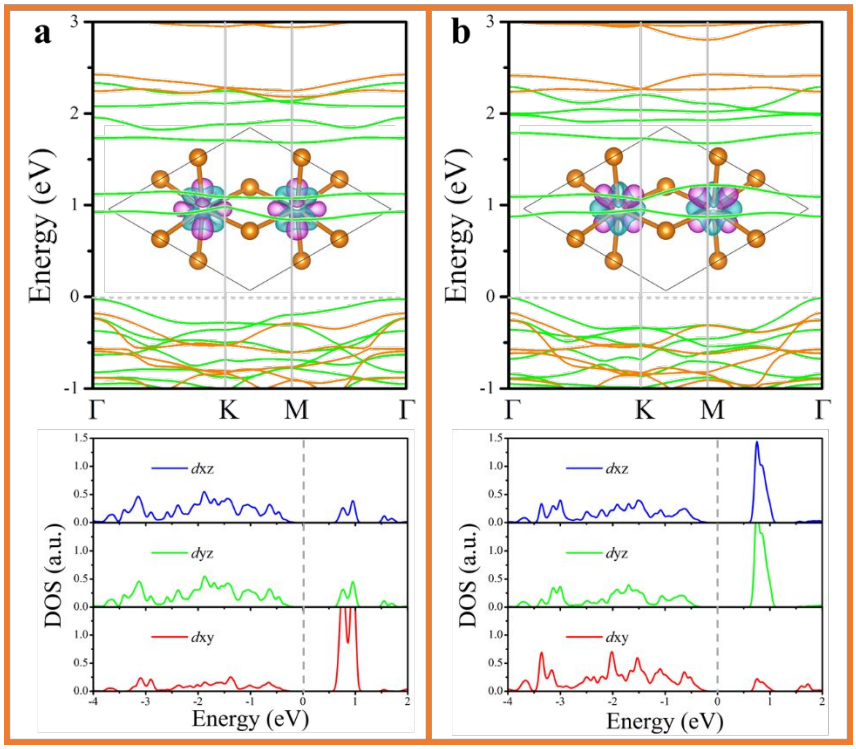

Fig. 3. Spin-resolved electronic band structures and partial density of states for (a) type-I and (b) type-II VI_3 monolayers. Green and orange lines represent spin-up and spin-down bands, respectively. Insets: spatial charge difference corresponding to the

high-symmetric D_{3d} phase, where blue and purple iso-surfaces represent charge increase and decrease, respectively.

The magnetic properties of the twin orbital-order phases are also different. Our calculations show that the magnetic ground states for type-I and type-II phases are both FM. But, due to symmetry reduction, the magnetic couplings of a certain V site to the three nearest neighboring V sites become inequivalent. The spin Hamiltonian can be written as

$$\hat{H} = -\frac{1}{2}\sum_i \left(J_1 \vec{S}_i \cdot \vec{S}_{i,1} + 2J_2 \vec{S}_i \cdot \vec{S}_{i,2}\right) - D\sum_i \vec{S}_{i,ez}^2,$$

where the summation i runs over all the V sites, J_1 (along [110] orientation) and J_2 (along [-210] and [210] orientation) represent two inequivalent nearest-neighbor exchange parameters, D is the single-ion magnetic anisotropic parameter, $S_{i,ez}$ represents the component of S_i along the direction of the easy-axis and $|\boldsymbol{S}| = 1$ for the d^2 V ions. The calculated J_1 and J_2 are respectively 4.7 and 5.6 meV for type-I phase, and 6.0 and 5.3 meV for type-II phase (see Fig. S6 in the Supporting Information[33] for details). Different from the experimentally observed bulk phases, the magnetic easy axis of VI_3 monolayer lies in-plane instead of out-of-plane. For type-I phase, the easy axis is along [110] orientation with magnetic anisotropic energies (MAE) of 2.1 and 1.7 meV corresponding to the [-110] and out-of-plane orientation, respectively. For type-II phase, the easy axis is along [-110] orientation, and the MAE corresponding to [110] and out-of-plane orientations are 1.0 and 0.6 meV, respectively. Such large magnetic anisotropy will allow the formation of long-range 2D FM order in VI_3 monolayer. As a result, our Monte-Carlo simulations confirm that both type-I and type-II phases exhibit FM order along their easy-axis directions below the Curie temperature, which are estimated to be ~33 and ~30 K (Fig. S6 in the Supporting

Information[33]), respectively, lower than that of the bulk phases (49~55 K [23]). This is similar to the CrI_3 case, in which the CrI_3 monolayer (~45 K) [20] also possess a lower T_C than its bulk (~61 K) [39].

3. Twin orbital-order phases in other VI_3-like systems

To examine the general applicability of the discussed mechanism of twin orbital-order effects, we also studied several other VI_3-like systems, namely the VCl_3 (d^2), NbI_3 (d^2) and $TiCl_3$ (d^1) monolayers (see Fig. S10 in the Supporting Information[33]). The results show that, in all these systems, two corresponding phases with opposite deformable directions and lowered crystal symmetry are also found. Despite small structural distortions, these phases are all semiconducting with sizable energy gaps. For NbI_3, the twin orbital-order phases are also very close in energy but the type-II phase is slightly preferred than the type-I phase. But for VCl_3, the type-I phase is much lower in energy than the type-II phase by 7.75 meV/atom, which might be due to its smaller super-exchange interactions because of the larger ionicity of V-Cl bonds. And for $TiCl_3$, the type-I phase is higher by 2.75 meV/atom than the type-II phase. Furthermore, same as VI_3 monolayer, the symmetry breaking in these systems are also highly related with the electronic correlation. When $U_{\text{eff}} = 0$ is used in the DFT+U calculations, the orbital ordering and structural distortion vanish, and the systems become metallic.

4. Difference between bulk and monolayer

Finally, we discuss the controversies about the low-energy phase for VI_3. First, the inter-atomic exchange interaction has been demonstrated to play an important role in determining the orbital ordering in this system. In the monolayer case, the intra-layer inter-atomic exchange interaction competes with the on-site splitting, resulting in competitive twin orbital-order phases. In the bulk case, due to the extra inter-layer interactions which further complicate the situation, the observed phases are reasonably different. Secondly, because of subtle structural distortions and small

transition barrier (< 5 meV) between equivalent JT states (Fig. S5b in the Supporting Information[33]), it would be difficult to determine or control the structural phases of VI_3.

Summary

In summary, studies of the VI_3 monolayer reveal that i) the orbital symmetry breaking and band gap opening are driven by strong electron correlation, suggesting that the VI_3 could be a FM Mott insulator; ii) the inter-atomic exchange interaction is relatively strong and competes with the on-site splitting; iii) as a result, two competing low-energy phases of VI_3 monolayer, namely the twin orbital-order phases, were discovered, which show different phase-dependent electric and magnetic properties. These phenomena were also discovered in other VI_3-like systems, implying a general but unusual electronic behavior in strongly correlated 2D systems. We are looking forward to experimental confirmation and realizations of twin orbital-order phases in VI_3-like 2D systems.

Supporting Information

The Supporting Information is available free of charge DOI: xxx.

Structural details of different VI_3 phases, the parameters derived from MLWFs results, relative energies for different VI_3 phases calculated by various methods, NEB calculations for ferroelectric switching of type-II phase and JT phase transition of type-I phase, calculation details of magnetic couplings and Monte-Carlo simulation results, carrier doping and strain effects, details of tight-binding cluster model analysis and results for other VI_3-like monolayers.

Acknowledgements

The work is supported by the NSFC (51522206, 11774173, 11474165), bthe Fundamental Research Funds for the Central Universities (No.30915011203), and by

the Outstanding Youth Fund of Nanjing Forestry University (NLJQ2015-03). C.H. and E.K. acknowledge the support from the Tianjing Supercomputer Centre and Shanghai Supercomputer Center. P.J. acknowledges partial supported from the U.S. Department of Energy, Office of Basic Energy Sciences, Division of Materials Sciences and Engineering under Award No.DE-FG02-96ER45579. We thank Hongjun Xiang, Junsheng Feng and Jinyang Ni from Fudan University and Jian Zhou from Xi'an Jiaotong University for valuable discussions.

References

1. M. Guennou, P. Bouvier, P. Toulemonde, C. Darie, C. Goujon, P. Bordet, M. Hanfland, and J. Kreisel, Jahn-Teller, Polarity, and Insulator-to-Metal Transition in $BiMnO_3$ at High Pressure. *Phys. Rev. Lett.* **2014**, 112, 075501.

2. J. E. Han, O. Gunnarsson, and V. H. Crespi, Strong superconductivity with local Jahn–Teller phonons in C_{60} solids. *Phys. Rev. Lett.* **2003**, 90, 167006.

3. Y. Ishikawa and Y. Syono, Giant Magnetostriction Due to Jahn-Teller Distortion in Fe_2TiO_4. *Phys. Rev. Lett.* **1971**, 26, 1335.

4. H. Liu and G. Khaliullin, Pseudo-Jahn-Teller Effect and Magnetoelastic Coupling in Spin-Orbit Mott Insulators. *Phys. Rev. Lett.* **2019**, 122, 057203.

5. I. B. Bersuker, Pseudo Jahn-Teller Origin of Perovskite Multiferroics, Magnetic-Ferroelectric Crossover, and Magnetoelectric Effects: The d^0-d^{10} Problem. *Phys. Rev. Lett.* **2012**, 108, 137202.

6. K. Xu and H. J. Xiang, Unusual ferroelectricity induced by the Jahn-Teller effect:

A case study on lacunar spinel compounds. *Phys. Rev. B* **2015**, 92, 121112.

7. Z. Wang, E. Ruff, M. Schmidt, V. Tsurkan, I. Kézsmárki, P. Lunkenheimer, and A. Loidl, Polar Dynamics at the Jahn-Teller Transition in Ferroelectric GaV_4S_8. *Phys. Rev. Lett.* **2015**, 115, 207601.

8. P. Barone, K. Yamauchi and S. Picozzi, Jahn-Teller distortions as a novel source of multiferroicity. *Phys. Rev. B* **2015**, 92, 014116.

9. C. Huang, Y. Du, H. Wu, H. Xiang, K. Deng, and E. Kan, Prediction of Intrinsic Ferromagnetic Ferroelectricity in a Transition-Metal Halide Monolayer. *Phys. Rev. Lett.* **2018**, 120, 147601.

10. J. Lu, W. Luo, J. Feng, and H. Xiang, Unusual Ferroelectricity in Two-Dimensional Perovskite Oxide Thin Films. *Nano Lett.*, **2018**, 18, 595–601.

11. J. Varignon, N. C. Bristowe, and P. Ghosez, Electric Field Control of Jahn-Teller Distortions in Bulk Perovskites. *Phys. Rev. Lett.* **2016**, 116, 057602.

12. L. M. Roth, Simple Narrow-Band Model of Ferromagnetism Due to Intra-Atomic Exchange. *Phys. Rev.* **1966**, 149, 306.

13. K. I. Kugel, and D. I. Khomskii, Crystal structure and magnetic properties of substances with orbital degeneracy. *Zh. Eksp. Teor. Fiz.* **1973**, 64, 1429.

14. E. Pavarini, E. Koch, and A. I. Lichtenstein, Mechanism for Orbital Ordering in $KCuF_3$. *Phys. Rev. Lett.* **2008**, 101, 266405.

15. E. Pavarini, and E. Koch, Origin of Jahn-Teller Distortion and Orbital Order in $LaMnO_3$. *Phys. Rev. Lett.* **2010**, 104, 086402.

16. A. Flesch, G. Zhang, E. Koch, and E. Pavarini, Orbital-order melting in rare-earth manganites: Role of superexchange. *Phys. Rev. B* **2012**, 85, 035124.

17. E. Pavarini, S. Biermann, A. Poteryaev, A. I. Lichtenstein, A. Georges, and O. K.

Andersen, Mott Transition and Suppression of Orbital Fluctuations in Orthorhombic $3d^1$ Perovskites, *Phys. Rev. Lett.* **2004**, 92, 176403.

18. W.-G. Yin, D. Volja, and W. Ku, Orbital Ordering in $LaMnO_3$: Electron-Electron versus Electron-Lattice Interactions. *Phys. Rev. Lett.* **2006**, 96, 116405.

19. K. Chang, J. Liu, H. Lin, N. Wang, K. Zhao, A. Zhang, F. Jin, Y. Zhong, X. Hu, W. Duan, Q. Zhang, L. Fu, Q.-K. Xue, X. Chen, and S.-H. Ji, Discovery of robust in-plane ferroelectricity in atomic-thick SnTe. *Science* **2016**, 353, 274-278.

20. B. Huang, G. Clark, E. Navarro-Moratalla, D. R. Klein, R. Cheng, K. L. Seyler, D. Zhong, E. Schmidgall, M. A. McGuire, D. H. Cobden, W. Yao, D. Xiao, P. Jarillo-Herrero, X. Xu, Layer-dependent ferromagnetism in a van der Waals crystal down to the monolayer limit. *Nature* **2017**, 546, 270–273..

21. C. Gong, L. Li, Z. Li, H. Ji, A. Stern, Y. Xia, T. Cao, W. Bao, C. Wang, Y. Wang, Z. Q. Qiu, R. J. Cava, S. G. Louie, J. Xia, X. Zhang, Discovery of intrinsic ferromagnetism in two-dimensional van der Waals crystals. *Nature* **2017**, 546, 265–269.

22. J. Xiao, H. Zhu, Y. Wang, W. Feng, Y. Hu, A. Dasgupta, Y. Han, Y. Wang, D. A. Muller, L. W. Martin, P. Hu, and X. Zhang. Intrinsic Two-Dimensional Ferroelectricity with Dipole Locking. *Phys. Rev. Lett.* **2018**, 120, 227601.

23. T. Kong, K. Stolze, E. I. Timmons, J. Tao, D. Ni, S. Guo, Z. Yang, R. Prozorov, and R. J. Cava, VI_3—a New Layered Ferromagnetic Semiconductor. Adv. Mater. **2019**, 31, 1808074.

24. S. Tian, J.-F. Zhang, C. Li, T. Ying, S. Li, X. Zhang, K. Liu, and H. Lei, Ferromagnetic van der Waals Crystal VI_3. *J. Am. Chem. Soc.*, **2019**, 141, 5326–5333.

25. S. Son et al. Bulk properties of the van derWaals hard ferromagnet VI_3. *Phys. Rev. B* **2019**, 99, 041402.

26. J. He, S. Ma, P. Lyua, and P. Nachtigall, P. Unusual Dirac half-metallicity with intrinsic ferromagnetism in vanadium trihalide monolayers. *J. Mater. Chem. C*, **2016**, 4, 2518.

27. C. Huang, J. Feng, F. Wu, D. Ahmed, B. Huang, H. Xiang, K. Deng, and E. Kan, Toward Intrinsic Room-Temperature Ferromagnetism in Two-Dimensional Semiconductors. *J. Am. Chem. Soc.*, **2018**, 140, 11519–11525.

28. G. Kresse, and J. Hafner, Ab initio molecular dynamics for liquid metals. *Phys. Rev. B* **1993**, 47, 558.

29. J. P. Perdew, K. Burke, and M. Ernzerhof, Generalized Gradient Approximation Made Simple. *Phys. Rev. Lett.* **1996**, 77, 3865.

30. P. E. Blöchl, Projector augmented-wave method. *Phys. Rev. B* **1994**, 50, 17953.

31. H. J. Monkhorst, and J. D. Pack, Special points for Brillouin-zone integrations. *Phys. Rev. B* **1976**, 13, 5188.

32. S. L. Dudarev, G. A. Botton, S. Y. Savrasov, C. J. Humphreys, and A. P. Sutton, Electron-energy-loss spectra and the structural stability of nickel oxide: An LSDA+U study. *Phys. Rev. B* **1998**, 57, 1505.

33. See Supporting Information, which includes Refs. (34-36).

34. A. A. Motofi, J. R. Yates, G. Pizzi, Y. S. Lee, I. Souza, D. Vanderbilt, and N. Marzari, An updated version of Wannier90: A Tool for Obtaining Maximally Localised Wannier Functions. *Comput. Phys. Commun*. **2014**, 185, 2309.

35. H. Katsura, N. Nagaosa, A. V. Balatsky, Spin Current and Magnetoelectric Effect in Noncollinear Magnets. *Phys. Rev. Lett.* **2005**, 95, 057205.

36. J. C. Slater, and G. F. Koster, Simplified LCAO Method for the Periodic Potential Problem. *Phys. Rev.* **1954**, 94, 1498.

37. A. Togo, and I. Tanaka, First principles phonon calculations in materials science. *Scr. Mater.* **2015**, 108, 1-5.

38. K. I. Kugel', and D. I. Khomskiĭ, The Jahn-Teller effect and magnetism: transition metal compounds. *Sov. Phys. Usp.* **1982**, 25, 231.

39. M. A. McGuire, H. Dixit, V. R. Cooper, and B. C. Sales, Coupling of crystal structure and magnetism in the layered, ferromagnetic insulator CrI_3. *Chem. Mater.* **2015**, 27, 612–620.

TOC

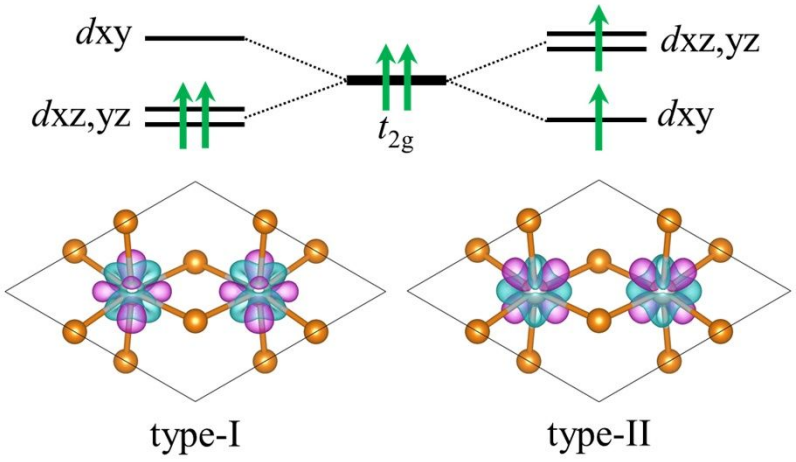

Discovery of twin orbital-order ferromagnetic semiconducting phases in VI_3-like 2D systems.